Integrative Biology

Accepted Manuscript

ROYAL SOCIETY OF CHEMISTRY

www.rsc.org/ibiology

Insight Statement

Curiously, this design prioritizes minimal cell-scaffold interactions, whereas cell-scaffold interactions are a ubiquitous part of liver biology. New materials-inspired strategies that induce the formation of cell aggregates with biologically relevant morphologies is a high priority. Here, we report the detailed investigation of hepatocarcinoma (Huh 7.5) cellular behavior in a collagen-functionalized microsphere-templated poly (ethylene glycol) (PEG) hydrogel scaffold which promotes 3D hepatic sheet morphology. Collagen conjugation led to improved liver-specific functions, including albumin production and cytochrome CYP450 activity. Importantly, the gene expression of numerous cell-adhesion markers was enhanced along with stimulated innate hepatocyte fibronectin production. The findings offer evidence that surface-coated collagen in the 3D hydrogel platform triggers the upregulation of hepatocyte-specific transcription factors and the secretion of liver metabolic markers.

Phenotypic Regulation of Liver Cells in a Biofunctionalized Three-Dimensional Hydrogel Platform

Myung Hee Kim [a,b], *Supriya K. Kumar*[a,b], *Hitomi Shirahama*[a,b], *Jeongeun Seo, Jae Ho Lee*[a,b], *Nam-Joon Cho*[a,b,c]*

[a]School of Materials Science and Engineering, Nanyang Technological University, 50 Nanyang Avenue 639798, Singapore
[b]Centre for Biomimetic Sensor Science, Nanyang Technological University, 50 Nanyang Avenue 639798, Singapore
[c]School of Chemical and Biomedical Engineering, Nanyang Technological University, 62 Nanyang Avenue 637459, Singapore

*Corresponding author. School of Materials Science and Engineering, Nanyang Technological University, 50 Nanyang Avenue 639798, Singapore Tel: +65 6592 7945; fax: +65 6790 9081
Email address: njcho@e.ntu.edu.sg (N.-J. Cho)

Abstract

Loss of function is a major challenge for hepatocytes that are cultured on two-dimensional (2D) cell culture platforms. Biofunctionalized three-dimensional (3D) scaffolds produced by microfabrication strategies can overcome these limitations by presenting vital environmental cues, strong mechanical properties, and a three-dimensional geometry to enable high-fidelity liver tissue engineering. Herein, we report the detailed investigation of hepatocarcinoma (Huh 7.5) cellular behavior in a collagen-functionalized microsphere-templated poly (ethylene glycol) (PEG) hydrogel scaffold which promotes 3D hepatic sheet morphology. Collagen conjugation led to improved liver-specific functions, including albumin production and cytochrome CYP450 activity. Importantly, the gene expression of numerous cell-adhesion markers was enhanced along with stimulated innate hepatocyte fibronectin production. Taken together, the findings reveal a close connection between hepatic cell morphology and gene expression, offering evidence that surface-coated collagen in the 3D hydrogel platform triggers the upregulation of hepatocyte-specific transcription factors and the secretion of liver metabolic markers.

Keywords:
Poly (ethylene glycol) (PEG) hydrogel; Inverted colloidal crystal (ICC); Cell-adhesion markers
Collagen conjugation; Hepatocyte culture; Microenvironment; Liver tissue engineering

1. Introduction

The liver is a critical organ, situated as part of the gastrointestinal tract, with an intricate microarchitecture and a broad range of key functions, including detoxification, xenobiotic metabolism, immunologic functions, and production and secretion of a multitude of proteins and bile constituents [1, 2]. Liver transplantation is the most effective therapy for patients with acute or chronic liver diseases and failure, but this therapeutic option is severely hindered by the shortage of liver supply [3]. Alternative treatments being developed include hepatocyte transplantation and extracorporeal bioartificial liver devices, both of which would require the proper culturing and maintenance of hepatocyte functions *in vitro* [2, 4].

Given the multifaceted microenvironment of the liver, the culture of hepatocytes on inadequate conventional two-dimensional (2D) substrates has resulted in loss of function and viability of the hepatocytes, especially over extended period of time [5-7]. The development of three-dimensional (3D) culture platforms and biomatrices for hepatocytes has proven superior and is able to overcome these aforementioned limitations, which are especially useful in the preclinical drug toxicity screening [8] and development of bioartificial liver support devices [4].

Current 3D microfabrication strategies and biomaterial constructs aim to mimic important aspects of the liver microarchitecture. Yarmush and his coworkers studied the viability and function of adult rat hepatocytes in a collagen sandwich culture, an extracellular matrix (ECM) configuration resembling that of the *in vivo* physiology [9-12]. Hepatocytes in the sandwich culture exhibited polygonal morphology in a monolayer formation and maintained liver-specific functions. This platform has been enhanced by altering the sandwich material flanking the hepatocyte cord [13] and inducing flow [8, 14, 15]. Bhatia and her team utilized tunable poly (ethylene glycol) (PEG)-based hydrogels to encapsulate hepatocytes for the study of increased cell-cell

interaction in microtissues [16], biodegradable synthetic hydrogels effect on hepatic function [17], and photo- and electropatterning to control the microenvironment more precisely [18]. Hydrogel-encapsulated co-cultured hepatocytes tended to form interconnected 3D cell networks and had prolonged function. Kotov and colleagues designed a hexagonally packed sphere-templated scaffold to promote 3D cell culture for multiple cell types, especially the formation of spheroids when culturing a hepatocarcinoma cell line (HepG2) in scaffolds made from nonfouling materials [19-23]. These highly ordered, mechanically stable, porous scaffolds promote cell-cell interaction and replenishment of nutrients and oxygen to the cells while removing secreted waste molecules. While spheroid culture has gained attention, its shortcomings include the presence of necrosis at the aggregates' center [24]; thereby conceding that different cell formations may show better results [25].

The goal of this study is to examine the synergistic effect of ECM presence and a highly ordered, porous scaffold on hepatocyte behavior. The composition of ECM proteins found in the *in vivo* physiology is specific to each tissue and regulates important cell behavior, such as cell adhesion, by interacting with integrins embedded in the cell membrane [26]. Collagen type I (Col I) is a prevalent ECM protein in the hepatic microenvironment [27, 28]. Therefore, we fabricated a Col I-functionalized PEG ICC microscaffold and seeded Huh-7.5 cells as our model hepatocyte cell line. The fabrication of the porous bioactive scaffold, ICC topology and the influence of the conjugated collagen concentration on Huh-7.5 cell growth and function were examined in detail.

2. Materials and Methods

2.1 Synthesis of PEG-Diacrylate (PEG-DA)

PEG-DA was synthesized according to previously published method without modification [29, 30]. Briefly, diol-terminated PEG (M_W = 4.6 kDa; Sigma-Aldrich, MO) was reacted with a 2.5 mol

excess of acryloyl chloride (Sigma-Aldrich) and triethylamine base catalyst in tetrahydrofuran (THF, Sigma-Aldrich) overnight at room temperature (RT). The resulting PEG-DA was then purified by filtration, liquid−liquid extraction in dichloromethane (Sigma-Aldrich) and precipitation in diethyl ether (Sigma-Aldrich).

2.2 PEGDA/PEG-NHS ICC scaffold

2.2.1 Fabrication of polystyrene (PS) colloidal crystal (CC)

An Eppendorf tube (I. D = 6 mm; Axygen Scientific, NY) glued to a microscope slide (Bioanalytic GmbH, Germany) was used as the CC mold. A suspension of PS spheres with a mean diameter of 140 μm (139 ± 2.9 μm; Duke Scientific, CA) in 70% ethanol (Merck, Germany) was pipetted into the molds and washed with ethanol (Merck). The assemblies were halfway immersed in an ultrasonic bath (Elma Schmidbauer GmbH, Germany) and sonicated for 2-3 min to arrange the individual spheres into ordered CCs of ~8-13 layers. After complete evaporation of ethanol at RT, the self-assembled CCs were sintered in a furnace at 130 ˚C for 6 h and removed from the molds.

2.2.2 Fabrication of PEGDA/PEG-NHS ICC scaffold

Hydrogel precursor solution, comprising either 50% *(w/v)* PEG-DA and 0.05% *(w/v)* photoinitiator (PI, 2-hydroxy-4'-(hydroxyethoxy)-2-methylpropiophenone; Sigma) or 50% *(w/v)* PEG-DA, 10% *(w/v)* Acryloyl-PEG-NHS (PEG-NHS; Laysan Bio, AL), and 0.05% *(w/v)* PI in deionized water, was infiltrated into the CCs by centrifugation. Excess prepolymer solution was removed by blotting. The infiltrated CCs were then exposed to 365 nm UV light (10.84 mW/cm^2) for 5 min and subsequently soaked in THF for 24 h to dissolve the PS spheres completely. Hydrogel scaffolds with the newly formed ICC pores were immersed in 70% ethanol

for 1 h, washed with phosphate buffered saline (PBS; Hyclone, UT; pH 7.4) with centrifugation to remove bubbles and sterilized under UV light for 30 min. **Fig. 1**A illustrates the scheme of the fabrication of PEG-based hydrogel ICC scaffolds.

2.2.3 Conjugation of Col I to PEG-NHS ICC scaffolds and visualization

PEG-NHS scaffolds (scaffolds that contain both PEG-DA and PEG-NHS) were surface-modified by Col I using amine-reactive crosslinker chemistry. Scaffolds were coated in either 20 μg/mL or 200 μg/mL solution of Col I from rat tail (Sigma; diluted in PBS), henceforth denoted Collagen 20 and Collagen 200 ICC scaffolds respectively, by centrifugation and shaking for 30 min and then incubated at 4 °C overnight.

To visualize the homogeneous coating with collagen, ICC scaffold were washed twice with PBS after the overnight collagen-conjugation, fixed with 4% paraformaldehyde (PFA; Alfa Aesar, MA) for 5 min, washed again with PBS and incubated with anti-mouse primary antibodies against Col I (1:100; Abcam) in 3% BSA overnight at 4°C. The samples were then washed three times with PBS and incubated with anti-mouse secondary antibody conjugated with Alexa Flour 488 (1:100; Life Technologies) for 2 h. Stained scaffolds were then imaged with LSM710 confocal and the 3D construction image was created by ZEN program.

2.2.4 Surface morphology of ICC scaffolds

Scanning emission microscopy (SEM) was employed to visualize the ordered cavities formed in the PEG-DA ICC scaffolds. Scaffolds were serially dehydrated in an ethanol solution and stored at -80 °C until ethanol evaporated completely. The samples were then dried in a Freezone 4.5 (Lobconco) freeze drier for 48 h, coated with a Pt film of 10 nm thickness using a JFC-1600 (JEOL) sputter coater and the micrographs were taken with a JSM-7600F (JEOL) FE-SEM instrument at a voltage of 5 kV.

2.3 Huh-7.5 cell culture and seeding

Prior to cell seeding, ICC scaffolds were placed in 24-well plates (Corning, NY), washed with PBS, and kept in 2 mL complete media for 30 min. Media was aspirated and scaffolds were dried for 1 h under UV light for sterilization. Huh-7.5 hepatocarcinoma cells (Apath) were maintained in Dulbecco's Modified Eagle's Medium (DMEM; Hyclone) supplemented with 10% fetal bovine serum (FBS; Hyclone), 100 U/mL penicillin (Life Technologies, MA) and 100 mg/mL streptomycin (Life Technologies, MA) at 37°C and 5% CO_2. One million cells in a 25 uL drop of media (4 x 10^7 cells/mL) was carefully pipetted on top of each ICC scaffold. After 12 h, cell-laden ICC scaffolds were transferred to new 24-well plates and media was changed every 3 days and maintained at 2 mL.

2.4 Cell-loading efficiency, viability and proliferation

Cell-loading efficiency was evaluated by quantifying the number of cells that adhered to the scaffold. On Day 1 post-cell seeding of the Huh-7.5 cells, cell-laden ICC scaffolds were transferred to another 24-well plate. Attached cell viability was analyzed quantitatively using the colorimetric Cell Counting Kit-8 (CCK-8; Dojindo Molecular Technologies, MD) according to the manufacturer's instructions. Concisely, cells were incubated with CCK-8 solution for 1 h at 37°C and the absorbance values (at λ = 450nm) of the collected media were measured using a Infinite® 200 PRO microplate reader (Tecan, Switzerland) [31, 32].

Spatial cell viability in ICC scaffolds was qualitatively assessed using the LIVE/DEAD® Cell Viability/Cytotoxicity kit (Life Technologies) according to manufacturer's protocol. Briefly, 4 μM calcein-AM and 8 μM ethidium homodimer-1 (EthD-1) were prepared in complete media, added to the cell-laden scaffolds and incubated for 1 h at 37 °C. The stained cells (green: live

cells [calcein], red: dead cells [EthD-1]) were visualized using a confocal microscope (LSM710, Carl Zeiss).

Cell proliferation was assessed using the CCK-8 assay on Days 1, 4, 7, 10 and 14 and normalizing measured absorbance values to Day 1 values for each condition. For later albumin secretion normalization, raw absorbance values were also converted to cell number using a standard curve.

2.5 Cell function and immunohistochemical staining

The amount of albumin secreted in media, collected every 3 days and stored at -80°C until use, was detected and quantified by human albumin enzyme-linked Immunosorbent assay (ELISA) kit (Abcam, UK). ELISA was performed according to the manufacturer's instructions. Data were normalized against the cell number and amount of albumin on Day 1.

For immunohistochemical analysis, albumin and CYP3A4 were stained to spatially visualize cell function of the hepatocytes in the 3D scaffolds on specific days. Huh-7.5-ICC scaffold constructs were washed twice with PBS, fixed with 4 % PFA for 5 min, permeabilized with 0.1 % Triton X-100 (Bio-Rad, CA) in PBS for 30 min, washed again with PBS and incubated in 3% BSA blocking buffer in PBS for 1 h. Cells were then incubated with anti-mouse primary antibodies against CYP3A4 or albumin (1:100; Santa Cruz Biotechnology, CA) overnight at 4 °C and then washed three times with PBS to remove unbound primary antibody. The cells were incubated with anti-mouse secondary antibody conjugated with Alexa Flour 488 (1:100; Life Technologies). At the same time, filamentous actin (F-actin) were stained with Alexa Flour 555 labelled phalloidin (Life Technologies) for 2 h at RT. After washing twice with PBS, cells in the ICC constructs were counterstained with 10 μg $mL^{=1}$ 2,6-diamidino-2-phenylinodole,

dihydrochloride (DAPI; Life Technologies) for 5 min and immediately images by confocal microscopy.

2.6 RNA extraction, reverse transcription and quantitative real time PCR

Isolation of total RNA, synthesis of cDNA, and quantitative real-time PCR was carried out as described previously [33]. To isolate RNA, the cell-laden ICC scaffolds were homogenized with TRIzol reagent (Life Technologies) and RNA concentration was measured using Nanodrop (Thermofisher Scientific; DE, USA). RNA was converted to cDNA through the synthesis of the first strand cDNA with iScript Reverse Transcription Supermix (Bio-Rad Laboratories, CA). Next, SYBR green–based real-time quantitative PCR (qPCR) was performed with the SYBR select Master Mix for CFX (Life Technology) in the CFX connect Real-Time PCR system using amplification mode (95 °C for 20 s, followed by 40 cycles of 10 s at 95 °C, and 40 s at 60 °C). The following genes were evaluated: (1) albumin; (2) alpha 1-antitrypsin (AAT); (3) glucose 6-phosphatase (G6P); (4) tyrosine aminotransferase (TAT); (5) cytrochrome 450 3A4 (CYP3A4); (6) cytochrome 450 3A7 (CYP3A7); (7) hepatocyte nuclear factor 4-alpha (HNF4α); (8) hepatocyte nuclear factor 6-alpha (HNF6α); (9) integrin beta-1 (Integrin β1); (10) E-cadherin; (11) N-cadherin; (12) hepatocyte cell adhesion molecule (hepaCAM); and (13) glyceraldehyde 3-phosphate dehydrogenase (GAPDH). Data were analyzed by the $2^{-\Delta\Delta CT}$ method, as described previously [34]. The detected levels of each gene mRNA were normalized against GAPDH. Primers were chosen with an online primer design program [35] and listed in Table 1.

Table 1. Primer sequences used in real-time PCR.

Target gene	Forward (5'-3')	Reverse (5'-3')
Albumin	CTGCACAGAATCCTTGGTGA	CTCCTTATCGTCAGCCTTGC
AAT	GATGCTGCCCAGAAGACAGA	GGAGTTCCTGGAAGCCTTCA
G6P	TTCCTGTTCAGCTTCGCCAT	TCAAAGACGTGCAGGAGGAC

TAT	GAGTCAGCGCATTTTGGGAC	ACTAACCGCTCCGTGAACTC
CYP3A4	ACCGTGACCCAAAGTACTGG	TTCAGGGGGATCTGTGTTTC
CYP3A7	AAGTGGACCCAGAAACTGCA	GGCTCCACTTACGGTCTCAT
HNF4α	TCGTTGAGTGGGCCAAGTAC	TGTCATCGATCTGCAGCTCC
HNF6	TTGAGCCATTGAGCGGACAT	GGCAGGTTCAAACGTTAGGC
Intergrin β	GAAGGGCGTGTTGGTAGACA	GTTGCACTCACACACACGAC
E-Cadherin	AGGCCAAGCAGCAGTACATT	AAATGTGTCTGGCTCCTGGG
N-Cadherin	CCTTTCAAACACAGCCACGG	TGTTTGGGTCGGTCTGGATG
hepaCAM	ATTTCGAGGCCACAGGTGTT	TCTCCACCATGCAGCTGTAC
GAPDH	CCATGGGGAAGGTGAAGGTC	CTCGCTCCTGGAAGATGGTG

2.7 Statistics

The statistical significance of differences between the groups was determined using the paired two-tailed student's t-test. Significance of gene expression was determined using GAPDH-normalized $2^{-\Delta\Delta CT}$ values. All data are represented as means ± SD. *, $p<0.05$; **, $p<0.01$; ***, $p<0.001$.

3. Results

3.1 Huh- 7.5 cell seeding in the highly ordered PEG-DA scaffolds with Col I-coating

PEG-based hydrogel ICC scaffolds were successfully fabricated using a self-assembled polystyrene (PS) colloidal crystal (CC) template. SEM micrographs show the packed hexagonal bead lattice, constructed from the PS spheres 140 μm in diameter, and the highly ordered and distinct pore cavities formed after PEG-DA hydrogel polymerization and particle leaching (**Fig. 1**B). The sphere size used and annealing time resulted in a mean pore and cavity interconnection diameter of 102 μm and 39 μm respectively, after dehydration of the scaffold. This porogen diameter was specifically chosen to limit the size and promote function of the hepatocyte spheroids [21], known to form in nonadhesive ICC scaffolds, thereby allowing proper penetration

of nutrients and oxygen to all Huh-7.5 cells. The 3D confocal image shows uniform conjugation of collagen along the surface of the porous scaffold (**Fig. 1**C).

After cell seeding, the Huh-7.5 cells were able to infiltrate the ICC scaffolds, settling into the cavities. The cell loading efficiency was evaluated in the PEG-DA scaffolds, with and without Col I conjugation, with an initial cell density of 1 x 10^6 cells per well (**Fig. 2**A). The seeding efficiency was significantly greater in the PEG-NHS ICC scaffolds and those coated with Col I in comparison to the bare PEG-DA scaffolds. The increased number of unattached cells in the bio-inert PEG-DA scaffold suggests both the Col I coating and presence of NHS ester promotes cell adhesion.

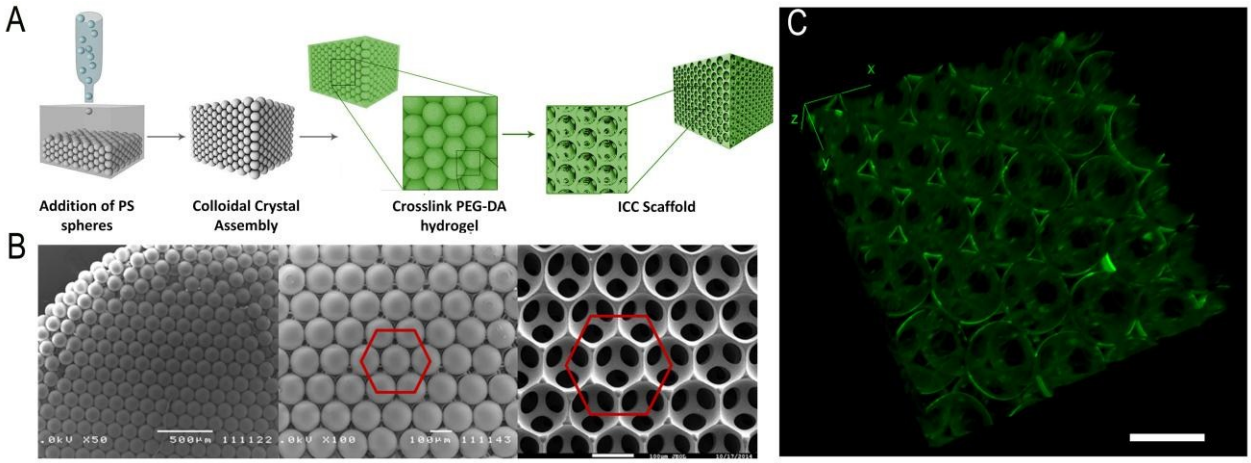

Figure 1. PEG-based hydrogel ICC scaffold. (A) Scheme of the ICC scaffold fabrication process. (B) SEM micrographs of self-assembled polystyrene (PS) bead lattices (left, middle; scale bars = 500 μm and 100 μm respectively) and an unseeded, highly ordered PEG-DA ICC scaffold (right; scale bar = 100 μm). (C) Confocal microscopy 3D image of collagen-conjugated ICC scaffold (scale bar = 200 μm). Green indicates the Col I stained by a specific Col I antibody.

3.2 Viability and proliferation of Huh-7.5 in Col-1 functionalized PEG-DA scaffolds

To understand the effect of ECM presence on Huh-7.5 growth within the ICC scaffolds, the cell proliferation, viability and organization were evaluated. Proliferation of the seeded Huh-7.5 cells, measured quantitatively by a colorimetric cell counting kit, was shown to notably increase in 3D scaffolds compared to the attenuated growth of cells on a 2D plastic culture plate (**Fig. 2**B). Among the 3D scaffolds, cells in the 200 μg/mL Col I coating demonstrated the steadiest proliferation through all 14 days of culture, whereas as the other three scaffolds showed a slight reduction on Day 14. By Day 14, this propagation value was approximately 2.5-fold higher than that of the 2D culture on Day 14.

Live/dead staining and confocal imaging showed that Huh-7.5 cells were highly viable in all scaffolds but showed marked differences in growth patterns (**Fig. 3**). In accordance with previous reports [21-23], the Huh-7.5 cells formed spheroids in the bare PEG-DA scaffolds and increased in diameter with the progression of time. Strikingly, the presence of the Col I coating directed the cells to line the cavity walls and these cell sheets then thickened and cell-cell interaction between cavities was visibly seen as early as day 1. Interestingly, the PEG-NHS scaffolds initially promoted cell adhesion to the pore surface, most likely through NHS ester-primary protein interaction, which supported the observed high seeding efficiency in **Fig. 2**A. However, this interaction was not strong enough and by Day 14, the cells start to detach slightly from the walls, and migrate to the center.

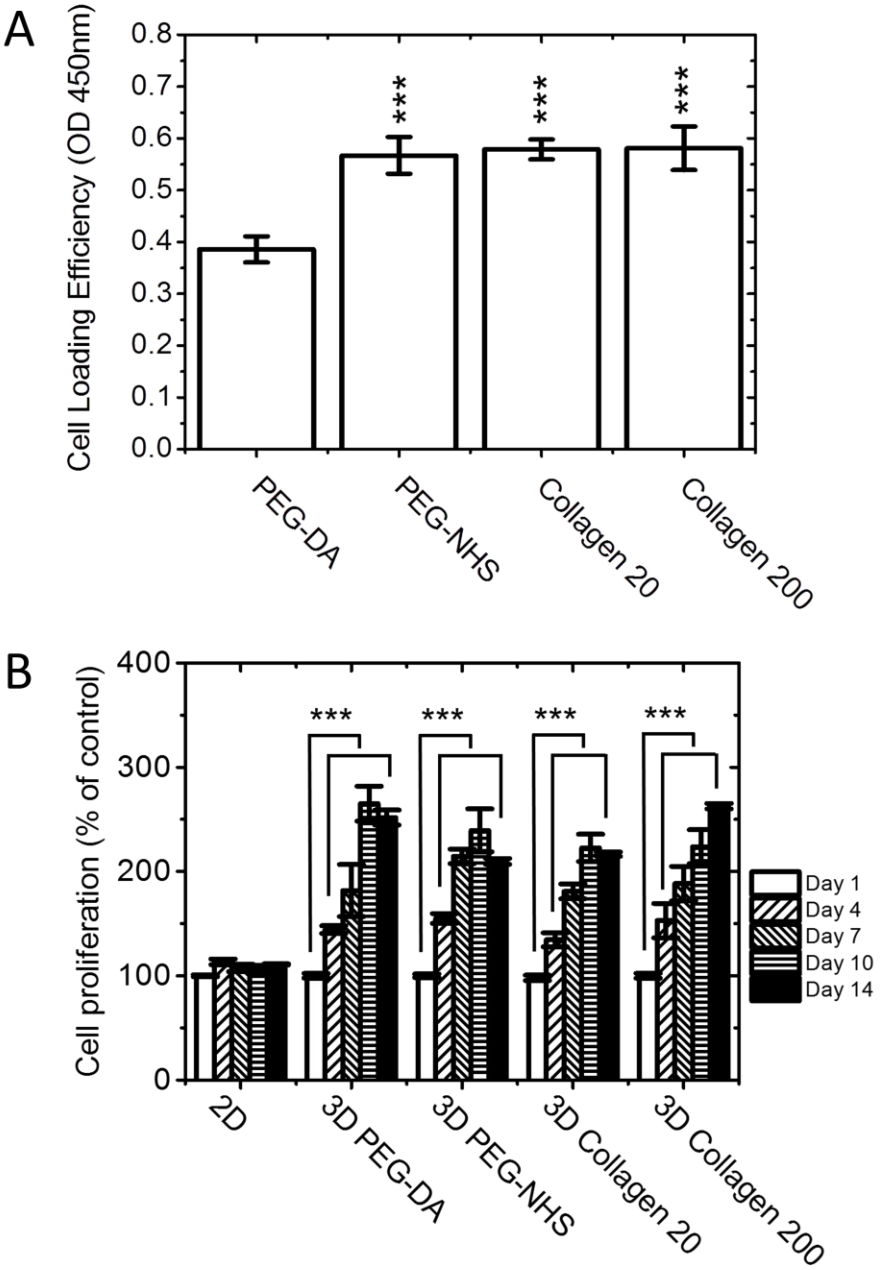

Figure 2. Effect of collagen conjugation and scaffold dimension on Huh-7.5 cell loading efficiency and proliferation. Huh-7.5 cells were seeded in 2D and/or 3D ICC scaffolds with or without conjugated Col I. (A) Cell loading efficiency was defined as the CCK-8 colorimetric assay spectrophotometer absorbance measurements on cells within the 3D ICC scaffolds 24 hrs post-cell seeding. (B) Cell proliferation was quantified by CCK-8 assay on 1,4,7,10, and 14 days post-cell seeding. The data were normalized to Day 1 absorbance values (Figure 2A). (n = 3, mean ± SD. *: $P < 0.05$. ** : $P < 0.01$ *** : $P < 0.001$ compared to CCK-8 absorbance reading for (A) PEG-DA group or (B) Day 1 of each group.)

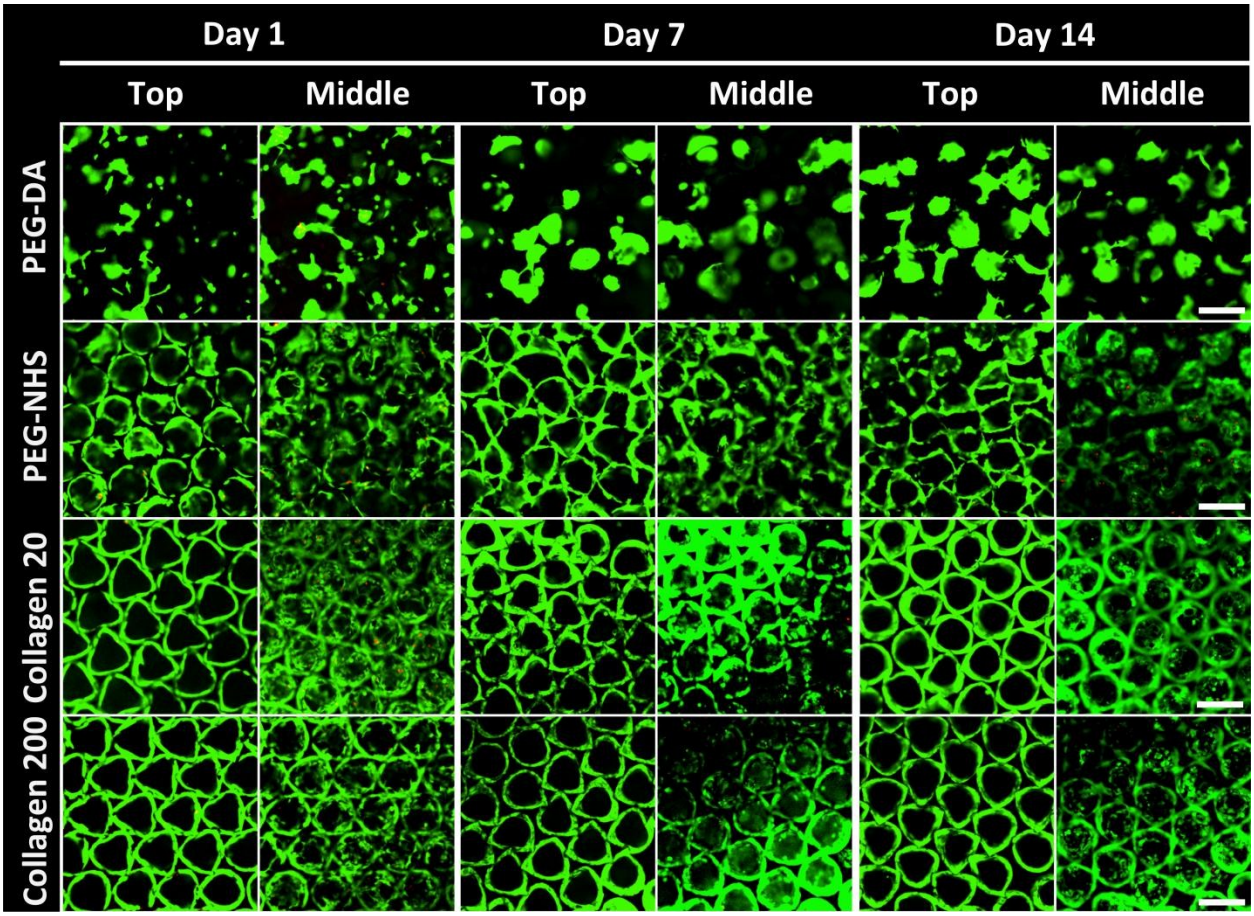

Figure 3. Evaluation of Huh-7.5 cell viability and growing pattern in 3D ICC scaffolds with and without conjugated Col I. Representative confocal z-stack images of Huh-7.5 cells after live/dead staining were taken near the top plane (z = 0-2 μm) and the middle plane (z = -30 μm) of an ICC scaffold spherical cavity (scale bars = 200 μm; image positions further explained in **Supplementary Data Fig. 1**). Green indicates live cells and red indicates dead cells.

3.3 Evaluation of Huh-7.5 albumin secretion and CYP3A4 activity in Col-1 functionalized PEG-DA scaffolds

Given the distinct Huh-7.5 growth patterns in PEG-DA ICC scaffolds with and without bioactive surface modification, metabolic activities specific to the liver were then assessed. During the first four days, the albumin secretion rates significantly increased in PEG-NHS and both collagen coated 3D ICC scaffolds (**Fig. 4**). With longer culture, the bare PEG-DA and PEG-NHS scaffold albumin secretion faltered while there was a parallel between the Col I conjugated concentration

and the albumin production rate. The ICC scaffold conjugated with 200 µg/mL displayed an albumin secretion rate approximately 1.5 times higher than the PEG-NHS ICC scaffold with and without 20 µg/mL conjugated Col I and 4times higher than the bare ICC scaffold. Further characterization of the Huh-7.5 cell behavior by immunohistochemical staining confirmed the morphological formation of the cells and revealed the spatial visualization of intracellular albumin (**Fig. 5A**) and CYP3A4 activity (**Fig. 5B**). Importantly, cell staining showed a high concentration of albumin and CYP3A4 activity in Huh-7.5 cells in collagen coated ICC scaffolds near the interconnections of the cavities, suggesting a dependence on the cell-cell interaction. Confocal images near the top of the scaffold showed a more even distribution of the plasma protein secretion and metabolic enzyme, but a higher activity again in the Col I conjugated ICC scaffolds (**Supplementary Data Fig. 2**A, B).

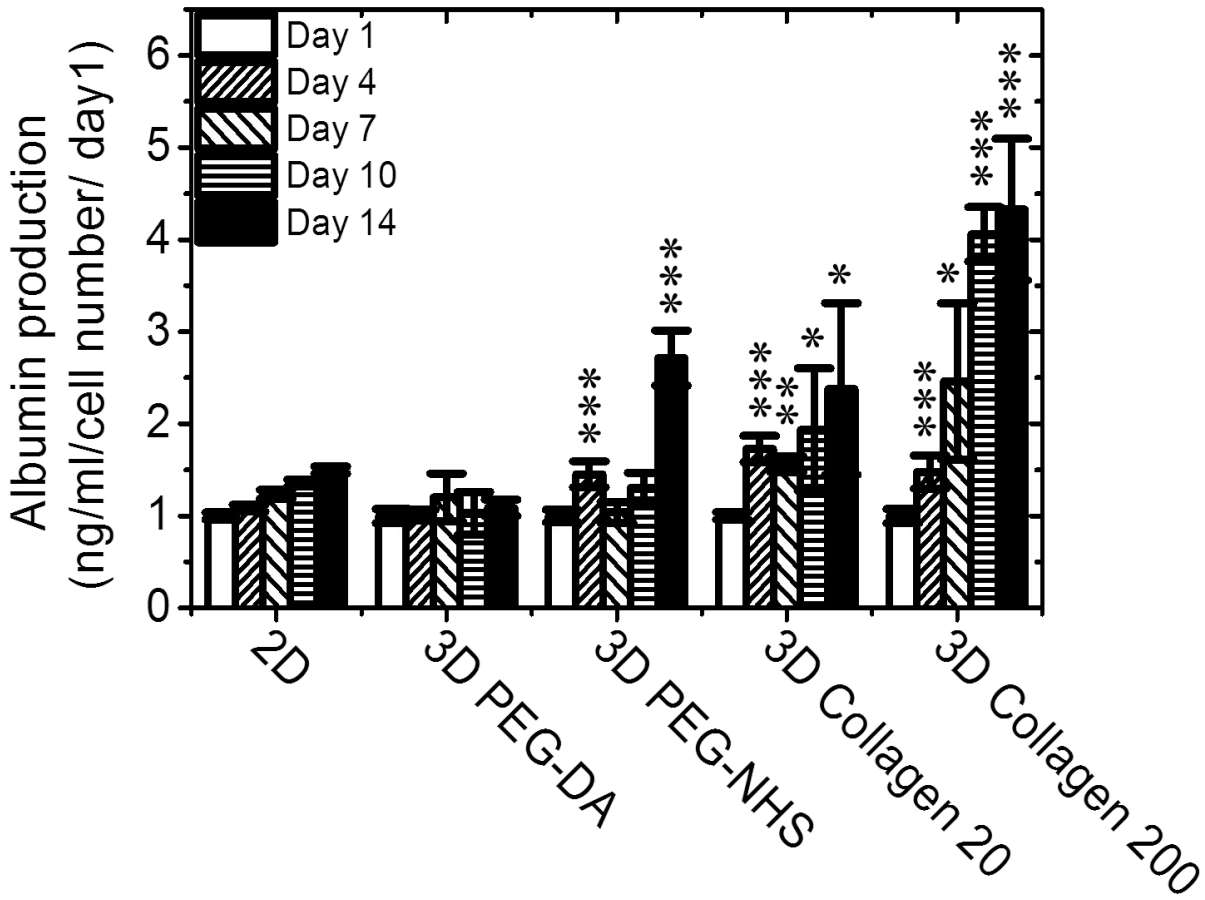

Figure 4. Evaluation of Huh-7.5 cell albumin secretion in 2D and/or 3D ICC scaffolds with or without conjugated Col I. Albumin secretion was measured from media samples collected on days 1, 4, 7, 10 and 14 by albumin ELISA for liver specific function. The data were normalized by cell number according to metabolism rate (refer to Figure 2B) and Day 1 values. (n = 3, mean ± SD; *: $P < 0.05$; ** : $P < 0.01$; *** : $P < 0.001$ compared to albumin production for day 1 of each group.)

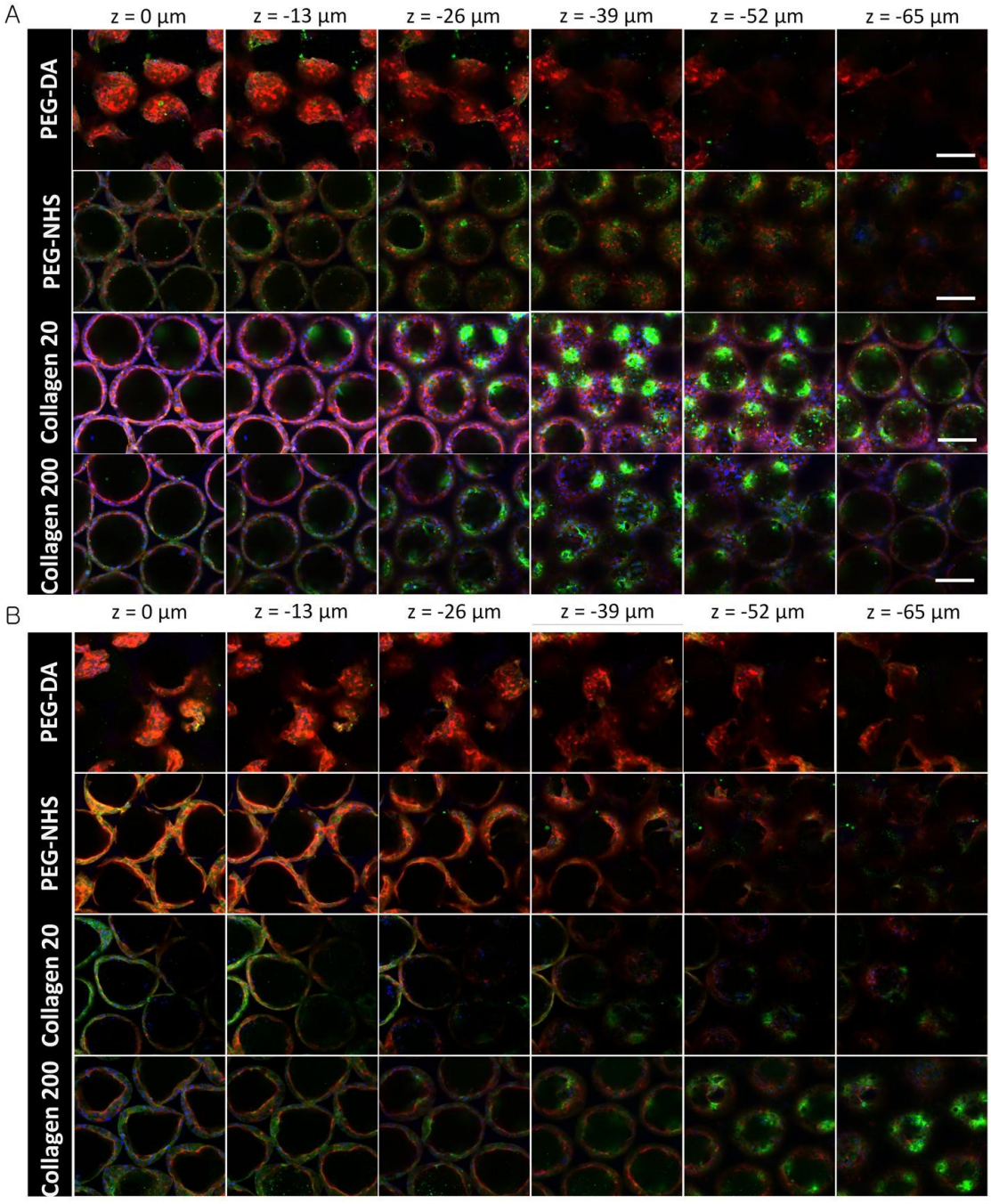

Figure 5. Evaluation of spatial liver specific function of Huh-7.5 cells by immunohistochemistry. Huh-7.5 cells were seeded in Col I coated or bare 3D ICC scaffolds and stained for F-actin (red), counterstained by DAPI for DNA (blue), and either stained for (A) albumin (green) on Day 7 or (B) CYP3A4 (green) on day 14. Representative confocal z-stack images show stained Huh-7.5 cells from the top (z = 0 µm) to interconnecting channel (z = -65 µm) of ICC scaffold spherical cavity in a serial manner (scale bars = 100 µm).

3.4 Hepatocyte-specific gene expression in Col I-functionalized PEG-DA scaffolds

In addition to a direct evaluation of hepatocyte phenotype, the effect of collagen conjugation on hepatocyte-specific gene expression was also quantified by RT-qPCR after total RNA extraction. The mRNA levels for AAT, and G6P, HNF6 and CYP3A4 were significantly up-regulated in a time-dependent manner while cultured in all ICC scaffolds, independent of the surface modification (**Fig. 6**A, B, D, E). However, other hepatocyte-specific genes, albumin and TAT, were markedly up-regulated in a dose-dependent manner of Col I on ICC ($p<0.05$, **Fig. 6**G, H). The highest induction in transcription factors such as HNF4 α and HNF6, which regulate the expression of liver secretory proteins [36] such as albumin [37], AAT [38], TAT [39] and G6P [40], was observed when multilayer cell sheets formed in the presence of 200 μg/ml collagen after 14 days (**Fig. 6**C, D). Similarly, CYP3A4 and CYP3A7, members of a cytochrome P450 subfamily involved in Phase I xenobiotic metabolism [41, 42], displayed the highest mRNA expression in the high dose Col I-conjugated ICC group (**Fig. 6**E, F).

In addition, as shown in **Fig. 3**, cell adhesion to the scaffold was significantly increased in collagen coated ICC scaffolds in comparison to the bare PEG-DA ICCs, suggesting that the presence of collagen promoted cell adhesion. To obtain more detailed molecular information about the transcriptional level of genes responsible for the improved cell adhesion, the expression of hepatocyte adhesion marker genes E- and N- cadherin [43], hepaCAM [44] and integrin β1 were analyzed (**Fig. 6**I-L). Huh-7.5 cells, which formed multilayer cell sheets in Col I-conjugated ICCs, exhibited an up-regulation of the four aforementioned hepatocyte-specific adhesion transcripts, especially E-cadherin and hepaCAM. In 2005, Moh et al. reported that hepaCAM is expressed in all normal and non-tumorous liver tissues and these molecules can

mediate the accelerated cell-matrix adhesion [44]. These data indicate that collagen markedly enhanced cell attachment by up-regulation of E cadherin and hepaCAM in 3D ICC platform.

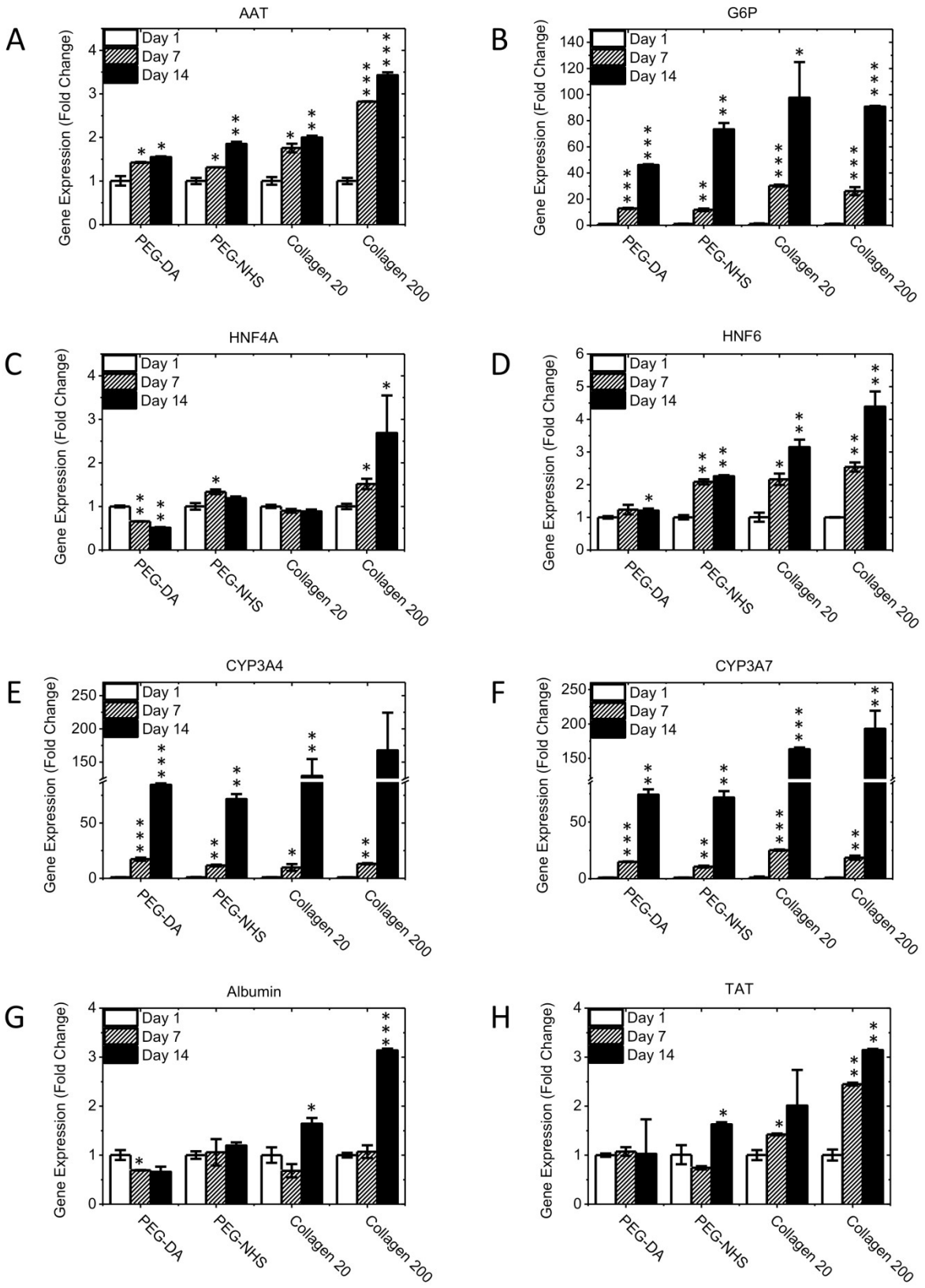

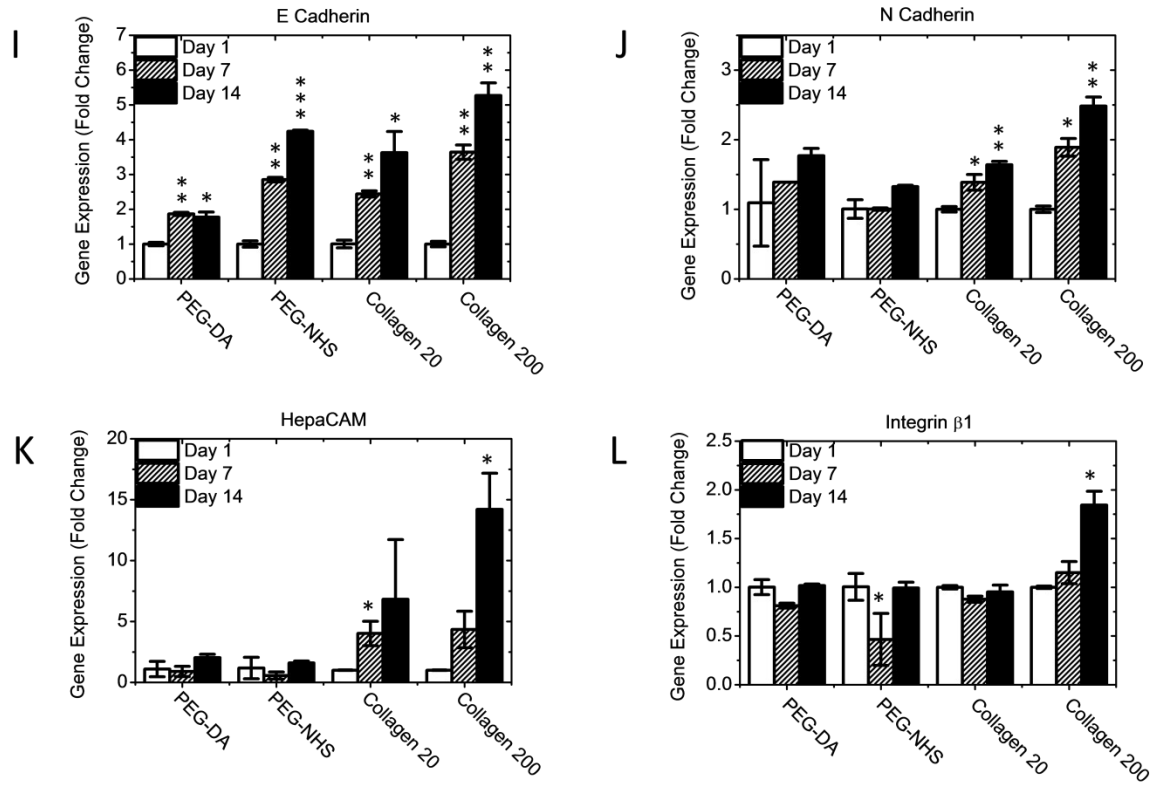

Figure 6. Effect of collagen conjugation on liver specific gene expression**.** Huh 7.5 cells were cultured in 3D ICC scaffolds with or without conjugated Col I, and RNA was extracted for the quantitative real-time PCR analysis of (A) alpha-1-antitrypsin (AAT), (B) glucose 6-phosphatase (G6P), (C,D) hepatocyte nuclear factors, (E,F) enzymes in the CYP3A subfamily of the CYP450 family (G) albumin, (H) tyrosine aminotransferase (TAT), and (I-L) cell adhesion proteins. The mRNA expression levels were normalized by GAPDH. (n = 3, mean ± SD; *: $P < 0.05$; ** : $P < 0.01$; *** : $P < 0.001$ compared to gene expression for Day 1 of each group.)

3.5 Secretion of ECM by Huh-7.5 in Col I-functionalized PEG-DA scaffolds

Lastly, to determine whether the presence of Col I on scaffolds affected the hepatocytes innate ability to remodel their surrounding ECM, Col I and fibronectin mRNA levels were quantified. The mRNA transcript levels indicate fibronectin was up-regulated in a time dependent manner and the highest expression was in the 200 µg/mL Col-I coated scaffolds (**Figure 7).** There is no apparent trend for the Col I profile based on the varied concentration of conjugated Col-I.

However, the increase in Col-I expression in 200 μg/mL Col-I conjugated scaffolds is significant at Day 14.

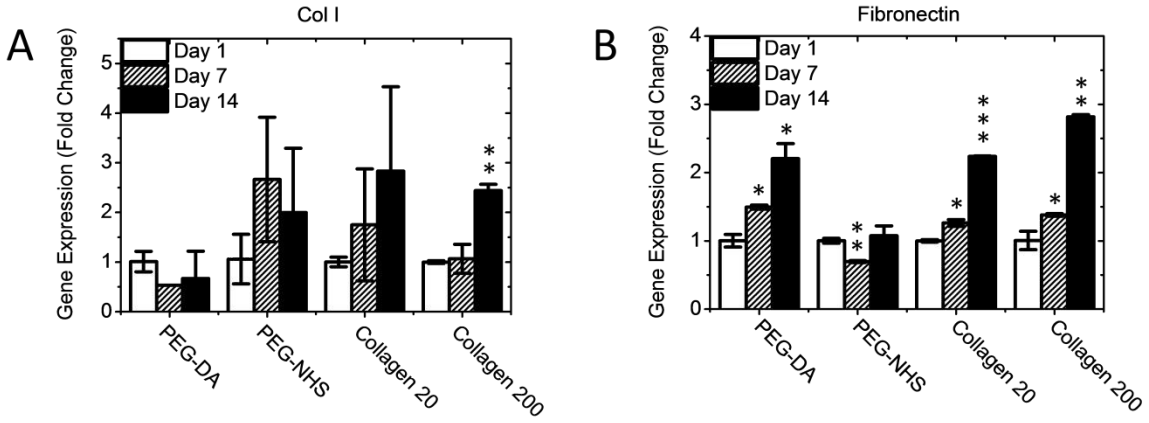

Figure 7. Effect of collagen conjugation on ECM gene expression. Huh 7.5 cells were cultured in 3D ICC scaffolds with or without conjugated Col I, and RNA was extracted for the quantitative real-time PCR analysis of (A) Col I and (B) fibronectin. The mRNA expression levels were normalized by GAPDH. (n = 3, mean ± SD; *: $P < 0.05$; ** : $P < 0.01$; *** : $P < 0.001$ compared to gene expression for Day 1 of each group.)

4. Discussion

One of the main challenges posed in liver tissue engineering is the design of an *in vitro* platform that will be able to maintain primary hepatocyte function over an extended period of time. The difficulty lies in the complexity of the native tissue architecture and the delicacy of the primary hepatocytes. The problem of acquiring and keeping primary hepatocytes has been temporarily bypassed by using model cells—inexpensive immortalized or carcinoma cell lines—that retain most of the hepatic functions with a few differences [45]. Great efforts and strides have been made to try and recreate the intricacies of the liver microarchitecture by combining various aspects of the hepatic microenvironment—ECM-presentation, co-culture, mechanical properties, geometry, chemical gradients and flow. Spheroid culture has been a promising technology, focusing on the scaffold geometry, because of the high diffusion properties and cell-cell interaction. However, given a limitation is the oxygen and nutrient penetration depth, the aggregation of cells above a

diameter of 150-200 μm [46] results in necrosis of cells present in the center. In the present study, we developed a biofunctionalized PEG hydrogel scaffold that combines geometry and collagen presence to direct the hepatocarcinoma cells into sheet morphology and enhance liver-specific functions.

The fabrication process, using PS spheres, yielded immaculately uniform interconnected cavities displaying the desired hexagonal structure (Fig. 1). Given the cavity size was approximately 102.3 μm (measured from the dehydrated SEM image of the scaffold), the hepatocyte spheroid in the base 3D PEG-DA scaffold had a diameter smaller than the critical value for necrosis and showed similar proliferation rates in comparison to the hepatocyte multi-sheet formation in collagen-conjugated scaffolds (Fig. 2). Interestingly, PEG-NHS scaffolds, without Col I conjugated, displayed signs of cell adhesion similar to that observed in collagen-conjugated scaffolds (Fig. 3). NHS esters have been shown to interact with the Lys residue that is prevalent on many proteins, including cell membrane proteins [47]. However after 7 days, the cells start to drift towards the center and aggregate there. Thus, it is to be noted the importance of cell adhesion strength in maintaining morphology integrity. The distinct cell growth pattern—multilayer cell sheet—in collagen-conjugated scaffolds could give rise to unique properties of the cultured cells versus spheroids in PEG-DA scaffolds[48].

Despite similar proliferation rates, the collagen-coated scaffolds displayed higher albumin secretion in a dose-dependent manner, highlighting the functional importance of cell-cell interactions and cell-ECM interactions. Importantly, the stark difference in formation of cell morphology led to differences in gene expression regulation. In conjunction with other liver-specific genes described in the results, Touboul et al. reported that TAT is also considered to be a marker of mature hepatocytes [39]. Also, Fu and colleagues demonstrated that TAT is a novel tumor

suppressor gene and its inactivation, caused by gene deletion and hypermethylation, contributes to the pathogenesis of hepatocellular carcinoma and this enzyme has the highest activity in the liver [49]. In this study, our results suggest that collagen potentially acts as a stimulator in 3D ICC by up-regulation of hepatocyte specific transcription factors (HNF6) and secretion of liver metabolic markers (especially TAT and AAT), when compared to culture in bare scaffolds.

In the broader context of ECM-cell interactions, it remains to be investigated whether other ECM proteins also promote liver-specific functions, as evidenced through similar gene expression profiles or otherwise. Indeed, it has long been suggested[50] that ECM-cell interactions could affect hepatic gene expression. Nagaki et al.[51] proposed that ECM components regulate gene expression by activating specific hepatic transcription factors, HNF-1 and HNF-4. Since then, multiple mechanisms have been reported but, to our knowledge, have not distinguished between the effects of different types of ECM proteins or combinations thereof on promoting liver-specific functions. Kimata et al.[52] more recently showed that there were differences in mRNA expression levels when cells were cultured on collagen type I, collagen type IV, laminin, or EHS gels and complex gels in a 2D culture system. Based on these findings, it would expected that there will be some differences in liver-specific functions depending on what ECM protein(s) is conjugated to the ICC scaffold. Collagen type I was chosen in our study because of its known importance and prevalence in the hepatic microenvironment, although there is significant potential to utilize the ICC platform for further exploring the functional effects of other ECM proteins as well.

5. Conclusions

ECM proteins play a significant role in regulating various cell behaviors, including cell adhesion, function, and migration among others. Using facile microfabrication techniques and EDC/NHS

chemistry, we combined two facets of the hepatic microenvironment, ECM presence and 3D geometry, to fabricate collagen-conjugated PEG-DA ICC scaffolds with porous topology for Huh-7.5 cell culture. Our results reveal the successful infiltration of cells into the bioactive scaffolds and the presence of collagen promoted cell-scaffold adhesion and cell-cell interaction, directing the cells into multilayer cell sheets that lined the cavity walls. In comparison to 2D cell platforms and 3D bare ICC scaffold culture, the Col I-conjugated hepatocyte culture enhanced cell proliferation, albumin secretion, CYP450 activity and up-regulated adhesion gene expression in addition to other liver-specific genes. This work shows the potential of this scaffold to be used in liver tissue engineering for the applications of tissue regeneration, xenobiotic toxicity studies, and disease study.

Acknowledgement

The authors wish to acknowledge support from a National Research Foundation Fellowship (NRF -NRFF2011-01) and Competitive Research Programme (NRF-CRP10-2012-07)

References

1. M. Müller and P. L. M. Jansen, *Journal of Hepatology*, 1998, **28**, 344-354.
2. S. N. Bhatia, G. H. Underhill, K. S. Zaret and I. J. Fox, *Sci Transl Med*, 2014, **6**, 245sr242.
3. K. A. Brown, *Curr Opin Gastroenterol*, 2005, **21**, 331-336.
4. C. Chan, F. Berthiaume, B. D. Nath, A. W. Tilles, M. Toner and M. L. Yarmush, *Liver Transpl*, 2004, **10**, 1331-1342.
5. M. Miyazaki, Y. Handa, M. Oda, T. Yabe, K. Miyano and J. Sato, *Exp Cell Res*, 1985, **159**, 176-190.
6. T. Croci and G. M. Williams, *Biochem Pharmacol*, 1985, **34**, 3029-3035.
7. M. H. Grant, M. A. Melvin, P. Shaw, W. T. Melvin and M. D. Burke, *FEBS Lett*, 1985, **190**, 99-103.
8. L. Xia, S. Ng, R. Han, X. Tuo, G. Xiao, H. L. Leo, T. Cheng and H. Yu, *Biomaterials*, 2009, **30**, 5927-5936.
9. J. Dunn, M. Yarmush, H. Koebe and R. Tompkins, *The FASEB Journal*, 1989, **3**, 174-177.
10. F. Berthiaume, P. V. Moghe, M. Toner and M. L. Yarmush, *The FASEB journal*, 1996, **10**, 1471-1484.
11. J. Dunn, R. G. Tompkins and M. L. Yarmush, *The Journal of cell biology*, 1992, **116**, 1043-1053.
12. J. C. Dunn, R. G. Tompkins and M. L. Yarmush, *Biotechnology progress*, 1991, **7**, 237-245.
13. S. Zhang, L. Xia, C. H. Kang, G. Xiao, S. M. Ong, Y. C. Toh, H. L. Leo, D. van Noort, S. H. Kan and H. H. Tang, *Biomaterials*, 2008, **29**, 3993-4002.
14. M. Hegde, R. Jindal, A. Bhushan, S. S. Bale, W. J. McCarty, I. Golberg, O. B. Usta and M. L. Yarmush, *Lab on a Chip*, 2014, **14**, 2033-2039.
15. G. D. Tan, G. W. Toh, E. Birgersson, J. Robens, D. van Noort and H. L. Leo, *Biotechnology and bioengineering*, 2013, **110**, 1663-1673.
16. C. Y. Li, K. R. Stevens, R. E. Schwartz, B. S. Alejandro, J. H. Huang and S. N. Bhatia, *Tissue Engineering Part A*, 2014.
17. K. R. Stevens, J. S. Miller, B. L. Blakely, C. S. Chen and S. N. Bhatia, *Journal of Biomedical Materials Research Part A*, 2015, n/a-n/a.
18. D. R. Albrecht, V. L. Tsang, R. L. Sah and S. N. Bhatia, *Lab on a Chip*, 2005, **5**, 111-118.
19. N. A. Kotov, Y. Liu, S. Wang, C. Cumming, M. Eghtedari, G. Vargas, M. Motamedi, J. Nichols and J. Cortiella, *Langmuir*, 2004, **20**, 7887-7892.
20. Y. Liu, S. Wang, J. W. Lee and N. A. Kotov, *Chemistry of Materials*, 2005, **17**, 4918-4924.
21. J. Lee, M. J. Cuddihy, G. M. Cater and N. A. Kotov, *Biomaterials*, 2009, **30**, 4687-4694.
22. J. Lee, G. D. Lilly, R. C. Doty, P. Podsiadlo and N. A. Kotov, *Small*, 2009, **5**, 1213-1221.
23. Y. Zhang, S. Wang, M. Eghtedari, M. Motamedi and N. A. Kotov, *Advanced Functional Materials*, 2005, **15**, 725-731.
24. R. M. Sutherland, *Science*, 1988, **240**, 177-184.
25. M. H. Kim, S. K. Kumar, H. Shirahama, J. Seo, J. H. Lee, V. P. Zhdanov and N.-J. Cho, *Macromolecular Bioscience*, 2015.
26. C. Frantz, K. M. Stewart and V. M. Weaver, *Journal of cell science*, 2010, **123**, 4195-4200.

27. S. Beken, K. Slaus, K. De Smet, M. Depreter, F. Roels, A. Vercruysse and V. Rogiers, *Toxicology in Vitro*, 1999, **13**, 571-577.
28. R. G. Wells.
29. D. J. Waters, K. Engberg, R. Parke-Houben, L. Hartmann, C. N. Ta, M. F. Toney and C. W. Frank, *Macromolecules*, 2010, **43**, 6861-6870.
30. D. L. Elbert and J. A. Hubbell, *Biomacromolecules*, 2001, **2**, 430-441.
31. J. Li, J. Pan, L. Zhang and Y. Yu, *Biomaterials*, 2003, **24**, 2317-2322.
32. C. Maslansky and G. Williams, *In Vitro Cell.Dev.Biol. -Plant*, 1982, **18**, 683-693.
33. S. Jeong, M. Rebeiz, P. Andolfatto, T. Werner, J. True and S. B. Carroll, *Cell*, 2008, **132**, 783-793.
34. K. J. Livak and T. D. Schmittgen, *Methods (San Diego, Calif.)*, 2001, **25**, 402-408.
35. S. Rozen and H. Skaletsky, *Methods in molecular biology (Clifton, N.J.)*, 2000, **132**, 365-386.
36. H. Nacer-Cherif, B. Bois-Joyeux, G. Rousseau, F. Lemaigre and J. Danan, *Biochem. J*, 2003, **369**, 583-591.
37. A. Kamiya, T. Kinoshita, Y. Ito, T. Matsui, Y. Morikawa, E. Senba, K. Nakashima, T. Taga, K. Yoshida and T. Kishimoto, *The EMBO journal*, 1999, **18**, 2127-2136.
38. G. A. Silverman, P. I. Bird, R. W. Carrell, P. B. Coughlin, P. G. Gettins, J. I. Irving, D. A. Lomas, C. J. Luke, R. W. Moyer and P. A. Pemberton, *Journal of Biological Chemistry*, 2001.
39. T. Touboul, N. R. Hannan, S. Corbineau, A. Martinez, C. Martinet, S. Branchereau, S. Mainot, H. Strick‐Marchand, R. Pedersen and J. Di Santo, *Hepatology*, 2010, **51**, 1754-1765.
40. R. C. Nordlie, J. D. Foster and A. J. Lange, *Annual review of nutrition*, 1999, **19**, 379-406.
41. K. Nakata, Y. TANAKA, T. Nakano, T. Adachi, H. TANAKA, T. KAMINUMA and T. ISHIKAWA, *Drug metabolism and pharmacokinetics*, 2006, **21**, 437-457.
42. C. P. Martinez-Jimenez, R. Jover, M. Teresa Donato, J. V. Castell and M. Jose Gomez-Lechon, *Current drug metabolism*, 2007, **8**, 185-194.
43. M. Takeichi, *Science*, 1991, **251**, 1451-1455.
44. M. C. Moh, L. H. Lee and S. Shen, *Journal of hepatology*, 2005, **42**, 833-841.
45. K. Anderson, L. Yin, C. Macdonald and M. H. Grant, *Toxicol In Vitro*, 1996, **10**, 721-727.
46. A. L. Harris, *Nature reviews. Cancer*, 2002, **2**, 38-47.
47. F. Chen, S. Gerber, V. M. Korkhov, S. Mireku, M. Bucher, K. P. Locher and R. Zenobi, *Journal of the American Society for Mass Spectrometry*, 2015, **26**, 493-498.
48. Y. Sakai, M. Koike, H. Hasegawa, K. Yamanouchi, A. Soyama, M. Takatsuki, T. Kuroki, K. Ohashi, T. Okano and S. Eguchi, *PLoS One*, 2013, **8**, e70970.
49. L. Fu, S. S. Dong, Y. W. Xie, L. S. Tai, L. Chen, K. L. Kong, K. Man, D. Xie, Y. Li and Y. Cheng, *Hepatology*, 2010, **51**, 1624-1634.
50. A. Ben-Ze'ev, G. S. Robinson, N. Bucher and S. R. Farmer, *Proceedings of the National Academy of Sciences*, 1988, **85**, 2161-2165.
51. M. Nagaki, Y. Shidoji, Y. Yamada, A. Sugiyama, M. Tanaka, T. Akaike, H. Ohnishi, H. Moriwaki and Y. Muto, *Biochemical and Biophysical Research Communications*, 1995, **210**, 38-43.
52. T. Kimata, M. Nagaki, T. Ogiso, T. Naiki, T. Kato and H. Moriwaki, *Hepatology*, 2006, **44**, 140-151.

Table of Contents: Graphical and Textual Abstract

Development of a biofunctionalized three-dimensional hydrogel scaffold for hepatoctye cell culture highlights the importance of cell morphology, more specifically sheet-layer formation, in regulating gene expression.